Phase behavior and bulk structural properties of a microphase former with anisotropic competing interactions: A density functional theory study

Daniel Stopper[*] and Roland Roth

Institute for Theoretical Physics, University of Tübingen, Auf der Morgenstelle 14, 72076 Tübingen, Germany

Using classical density functional theory, we investigate systems exhibiting interactions where a short-range anisotropic attractive force competes with a long-range spherically symmetric repulsive force. The former is modelled within Wertheim's first-order perturbation theory for patchy particles, and the repulsive part is assumed to be a Yukawa potential which is taken into account via a mean-field approximation. From previous studies of systems with spherically symmetric competing interactions, it is well known that such systems can exhibit stable bulk cluster phases (microphase separation) provided that the repulsion is sufficiently weak compared to the attraction. For the present model system, we find rich phase diagrams including both reentrant clustering and liquid-gas binodals. In particular, the model predicts inhomogeneous bulk phases at extremely low packing fractions, which cannot be observed in systems with isotropic competing interactions.

I. INTRODUCTION

The interactions between particles in soft-matter systems cover a wide range of characteristics. The probably simplest yet most important reference system of hard spheres has been extensively studied for more than half a century in statistical physics because it governs essential features of the liquid and crystal phase [1]. Its properties are well described by integral equations [2,3], computer simulations (i.e., molecular-dynamics or Monte Carlo methods) [4], or classical density functional theory (DFT) [5–7]. Moving up a degree in complexity, particles interacting via a hard-core and a longer-ranged spherical attractive tail give rise to gas-liquid phase separation, and it is possible to study a variety of phenomena, e.g., the interface between two or more coexisting phases or wetting phenomena at attractive substrates [8].

However, some years ago, experimentally, the self-assembly of diblock copolymers into complex three-dimensional mesoscopic cluster phases was observed, including lamellar, cylindrical, and gyroid phases [9]. This behavior could not been rationalized with a pure attraction between the particles and indeed was traced back to a complex interplay between an attraction on short and a (weaker) repulsion on larger distances [10,11]. Later, Ciach *et al.* predicted via a Landau-type theory that also a colloidal suspension, where particles are assumed to interact via spherically symmetric competing interactions in addition to a hard-core repulsion, may be able to self-assemble into such microphases [12].

Systematic theoretical studies of model colloidal systems with competing interactions were done first by Gelbart [13] and Reatto [14]. By means of computer simulations and a random-phase approximation for the bulk pair direct correlation function $c(|\mathbf{r} - \mathbf{r}'|)$, they showed that for a small but nonzero wave number k_c a diverging peak in the static structure factor $S(k)$ emerges at the locus in the phase diagram where microphase separation occurs, indicating an instability of the homogeneous bulk phase against arbitrary small fluctuations.

Various subsequent studies employing both DFT as well as computer simulations have extensively addressed questions related to structure and thermodynamics [15,16], or the nature of the phase transition from the homogeneous towards a microphase-separated bulk state [17,18]. In particular, very recently both a DFT and a Monte Carlo simulation study showed that model colloidal suspensions with competing interactions indeed can self-assemble into complex structures including lamellar, 2D hexagonal, and gyroid structures [19,20]. Furthermore, effects of spherically competing interactions have been investigated in two dimensions [21] or for mixtures of soft particles [22]. However, in experiments it turns out to be challenging to fine-tune colloidal interactions sufficiently, so that self-assembly into ordered clusters has not been observed yet (see Ref. [23] and references therein for an overview of recent advances of model colloidal systems with competing interactions). Nevertheless, it is interesting to note that, e.g., gyroid structures are realized in nature in photonic crystals, e.g., in bird feathers [24] or butterfly wings [25], where they are responsible for structural colors.

While all these studies have in common that they assume spherically symmetric interactions, there are numerous situations in which anisotropic interactions are present in experimental systems such as globular proteins in solution [26–28], colloidal clays [29], or protein-salt mixtures [30]. Such highly directional interactions can properly modelled using the framework of patchy particles [26,29–31]. In that model, in addition to a hard core, the particles have attractive sites distributed on their surface, and they attract each other only if they are in a sufficient distance and are orientated correctly. In particular, Wertheim has developed a successful thermodynamic perturbation theory [32,33] for patchy particles, where in many situations it suffices to consider its first-order contribution (TPT1). The resulting thermodynamic bulk properties and phase diagrams are in reasonably good agreement with simulations [33], and, importantly, TPT1 is capable of predicting essential features of patchy particles, including phenomena such as empty liquids [29,34,35] or reentrant gas-liquid phase separation [36,37]. A broad overview of current (bulk) perspectives regarding patchy particles can be found in Ref. [31].

———————
[*]daniel.stopper@uni-tuebingen.de

Importantly, both homogeneous and inhomogeneous versions of Wertheim theory have been incorporated into the framework of DFT. While the latter has been shown to overestimate peak heights and contact densities at a hard wall, a DFT developed by Segura *et al.* based on the homogeneous form, i.e., where the bulk density ρ is replaced by an averaged local density, yields proper results even at high densities [38]. More importantly, the latter has been formulated within the framework of Rosenfeld's fundamental measure theory (FMT) [6,7] by Yu and Wu [39], and it provides quantitatively reliable results in comparison to computer simulations even at high particle densities and relatively strong association for the case of four patches per particle. In numerous studies, the theory successfully has been applied in order to investigate liquid-gas interfaces of patchy colloids [40], the confinement in slitlike pores [41], or a density functional theory study for water [42], just to mention a few. However, it is important to note that so far any kind of DFT for patchy particles neglects the orientational character of the interaction, which is accurate in the bulk phase, but in inhomogeneous situations, e.g., close to a hard wall, particle orientations can become relevant. Indeed, while in systems with four patches the orientational dependence properly averages out due to symmetry, a recent study revealed that in the case of strong association between the particles common DFT formulations fail to capture fundamental properties of the density distribution at a hard wall for particles with three patches [43].

Here we provide a DFT study for systems consisting of particles with a hard-core diameter σ possessing an anisotropic attraction via four patches and an additional Yukawa-type repulsion at larger distances. The hard-core and patchy interaction are modelled within the framework of FMT, and the repulsive tail is treated with a standard mean-field approach [1]. In Sec. II we introduce the theory covering the model system (Sec. II A) and give a brief introduction to DFT (Sec. II B), and finally we discuss details regarding the static structure factor $S(k)$ in Sec. II C. In Sec. III we focus on thermodynamic bulk properties and phase diagrams. Subsequently, in Sec. IV, we study the bulk structure of the system, where we find that the behavior of the phase diagrams is reflected in terms of the inhomogeneous density distribution $\rho(\mathbf{r})$ in an intriguing way. In Sec. V we focus on the question what kind of microphases can be stable within the region of instability, and we compare our results to previous studies of spherically symmetric competing interactions. Finally, we give a discussion and conclusion as well as possible applications to experimental systems of the model in Sec. VI.

II. THEORETICAL FRAMEWORK

A. Model system

In order to model anisotropic competing interactions we choose the pair interaction potential to be a composition of the Kern-Frenkel [44] and a spherically symmetric repulsive Yukawa potential. Specifically, the total pair-interaction potential between two particles 1 and 2 is given by

$$\phi(\mathbf{r},\Omega_1,\Omega_2) = \phi_{\rm hs}(r) + \phi_{\rm r}(r) + \phi_{\rm bond}(\mathbf{r},\Omega_1,\Omega_2) \quad (1)$$

where $\phi_{\rm hs}(r)$ is the usual hard-sphere potential, $r = |\mathbf{r}| \equiv |\mathbf{r}_1 - \mathbf{r}_2|$ is the center-to-center distance between particles 1
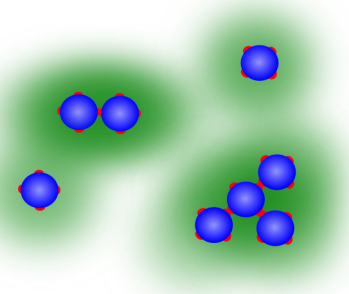
FIG. 1. Schematic illustration of the model system. Patchy particles (blue) with four attractive sites (red) and an additional spherical Yukawa-type repulsion (green).

and 2, and Ω_i denote individual orientation vectors. The Yukawa potential has the form ($r \geqslant \sigma$)

$$\phi_{\rm r}(r) = B\frac{\sigma}{r} \exp\left[-z(r/\sigma - 1)\right], \quad (2)$$

where B controls the contact value at $r = \sigma$ and z the range of repulsion. Furthermore, $\phi_{\rm bond}(\mathbf{r},\Omega_1,\Omega_2)$ is given by

$$\phi_{\rm bond}(\mathbf{r},\Omega_1,\Omega_2) = \phi_{\rm sw}(r) \cdot \sum_{\alpha,\beta} G(\hat{\mathbf{r}},\hat{\mathbf{r}}_1^\alpha(\Omega_1),\hat{\mathbf{r}}_2^\beta(\Omega_2)), \quad (3)$$

in which

$$\phi_{\rm sw}(r) = \begin{cases} -\varepsilon & \text{if } \sigma < r < \lambda\sigma \\ 0 & \text{otherwise} \end{cases} \quad (4)$$

describes a square-well interaction between two sites. The parameter λ controls the range of the attraction, and ε is the potential depth, which we assume to be identical for all patches. The function G contains the orientational character of the interaction,

$$G\left(\hat{\mathbf{r}},\hat{\mathbf{r}}_1^\alpha(\Omega_1),\hat{\mathbf{r}}_2^\beta(\Omega_2)\right) = \begin{cases} 1 & \text{if } \begin{cases} \hat{\mathbf{r}} \cdot \hat{\mathbf{r}}_1^\alpha > \cos(\theta_c), \\ -\hat{\mathbf{r}} \cdot \hat{\mathbf{r}}_2^\beta > \cos(\theta_c), \end{cases} \\ 0 & \text{else}, \end{cases}$$

$$(5)$$

where $\hat{\mathbf{r}} = (\mathbf{r}_1 - \mathbf{r}_2)/|\mathbf{r}_1 - \mathbf{r}_2|$ denotes the center-to-center unit vector between particles 1 and 2, and $\hat{\mathbf{r}}_i^\alpha$ is a unit vector from the center of particle i to a patch α on its surface depending on the individual orientation Ω_i. Hence, the product of $\phi_{\rm sw}$ and G accounts for the anisotropic character of the interaction; it is attractive only if two patches are within a sufficient distance and are orientated to each other properly, depending on the patch opening angle θ_c. A schematic illustration of the model system is pictured in Fig. 1.

Bond formation between particles is adequately described by Wertheims first-order perturbation theory [32,45–47]. For M identical patches, the contribution $f_{\rm bond}$ to the free-energy density of the bulk system can be written as [33]

$$\beta f_{\rm bond} = \rho M\left[\ln(X) - \frac{X}{2} + \frac{1}{2}\right], \quad (6)$$

where $\rho = N/V$ denotes the number density, $\beta = 1/(k_B T)$ the inverse temperature, and X is the probability that an arbitrary patch is *not* bonded. For the present case of a

one-component system with identical patches, X is given by the following mass-action equation:

$$X = \frac{1}{1 + \rho M X \Delta}, \qquad (7)$$

in which Δ is a measure for the interaction between two patches and reads [33]

$$\Delta = \int d\mathbf{r} \, g_R(r) \langle \exp(-\beta \phi_{\text{bond}}) - 1 \rangle_{\Omega_1, \Omega_2}$$
$$\approx \pi \sigma^3 g_R(\sigma^+)[\exp(\beta \varepsilon) - 1](1 - \cos(\theta_c))^2 (\lambda - 1), \quad (8)$$

connecting all geometrical and physical quantities of the patches, and $\langle \cdot \rangle_{\Omega_1, \Omega_2}$ denotes an angular average over all orientations of particles 1 and 2. Furthermore, the radial distribution function $g_R(r)$ of the reference system has been approximated by its contact value $g_R(\sigma^+)$, due to the short range of the site-site interaction. For the present model, strictly speaking the reference system would be the repulsive Yukawa fluid. However, we approximate the latter using the Carnahan-Starling expression for the pure hard-sphere system, $g_R(\sigma^+) \approx g_{\text{hs}}(\sigma^+) = (1 - \eta/2)/(1 - \eta)^3$, where $\eta = \pi \sigma^3 \rho/6$ is the fluid packing fraction. For completeness, we note that a first-order mean spherical approximation for $g_R(\sigma^+)$ for Yukawa systems is available [48], but its usage only slightly affects the resulting bulk phase diagrams shown in Sec. III. In the present work we employ $\lambda = 1.1$ and $\theta_c = 27°$, where these values ensure that the single-bond condition per patch is satisfied as assumed by TPT1. Note further that ring formation is not accounted for within the first-order description, but can be included in higher-order expansions [33].

B. Density functional theory

In order to investigate structure and thermodynamic properties such as pressure, thermal compressibility, or bulk phase behavior on equal footing, density functional theory (DFT) [5] provides a powerful and well-established framework. In DFT one minimizes the grand potential functional $\Omega[\rho]$ w.r.t. the one-body density profile $\rho(\mathbf{r})$ in order to obtain the equilibrium particle distribution $\rho_0(\mathbf{r})$, and $\Omega = \Omega[\rho_0(\mathbf{r})]$ is the grand potential of the fluid. The grand potential functional is given by

$$\Omega[\rho] = F_{\text{id}}[\rho] + F_{\text{ex}}[\rho] + \int d\mathbf{r} \, \rho(\mathbf{r})[V_{\text{ext}}(\mathbf{r}) - \mu], \quad (9)$$

where $V_{\text{ext}}(\mathbf{r})$ is an arbitrary external field and μ denotes the chemical potential of the particle reservoir. The quantity $F_{\text{id}}[\rho]$ is the free-energy functional of the ideal gas, which is known analytically,

$$\beta F_{\text{id}}[\rho] = \int d\mathbf{r} \, \rho(\mathbf{r})\{\ln[\Lambda^3 \rho(\mathbf{r})] - 1\}, \quad (10)$$

in which Λ denotes the thermal wavelength. The excess part $F_{\text{ex}}[\rho]$ contains information about the particle interactions, and in general this quantity is not known exactly (this would be equivalent having access to the partition sum), and therefore approximations have to be made. For the present system, we describe the hard-sphere and bonding contribution within the framework of fundamental measure theory (FMT) [6,7],

whereas the long-range repulsion is taken into account via a first-order perturbation theory [1],

$$\beta F_{\text{ex}}[\rho] = \int d\mathbf{r} \, [\Phi_{\text{hs}}(\{n_\alpha\}) + \Phi_{\text{bond}}(\{n_\alpha\})] + \frac{1}{2} \iint d\mathbf{r} \, d\mathbf{r}'$$
$$\times \rho(\mathbf{r})\rho(\mathbf{r}')g_{\text{hs}}(\mathbf{r},\mathbf{r}')\beta \phi_{\text{r}}(|\mathbf{r} - \mathbf{r}'|). \quad (11)$$

The last term is further simplified by assuming that the radial distribution function of hard spheres is $g_{\text{hs}}(\mathbf{r},\mathbf{r}') \approx 1$ in the range of the repulsive interaction; since in this work we consider a rather long-ranged repulsion of several particle diameters, and the considered fluid packing fractions are relatively small, we expect the approximation to be (at least) qualitatively reliable.

For the hard-sphere interaction, we employ the accurate White-Bear mark II functional [49],

$$\Phi_{\text{hs}}(\{n_\alpha\}) = -n_0 \ln(1 - n_3) + (n_1 n_2 - \mathbf{n}_1 \cdot \mathbf{n}_2)\frac{1 + \frac{1}{3}\chi_2(n_3)}{1 - n_3}$$
$$+ (n_2^3 - 3n_2 \mathbf{n}_2 \cdot \mathbf{n}_2)\frac{1 - \frac{1}{3}\chi_3(n_3)}{24\pi(1 - n_3)^2}, \quad (12)$$

in which the functions χ_2 and χ_3 are given by

$$\chi_2(n_3) = \frac{1}{n_3}\big[2n_3 - n_3^2 + 2(1 - n_3)\ln(1 - n_3)\big],$$

$$\chi_3(n_3) = \frac{1}{n_3^2}\big[2n_3 - 3n_3^2 + 2n_3^3 + 2(1 - n_3)^2 \ln(1 - n_3)\big]. \quad (13)$$

The weighted densities $n_\alpha(\mathbf{r})$ are defined as convolutions of the density $\rho(\mathbf{r})$ with certain weight functions $\omega_\alpha(\mathbf{r})$ describing the fundamental geometries of a sphere [6],

$$n_\alpha(\mathbf{r}) = \int d r' \, \rho(\mathbf{r}')\omega_\alpha(\mathbf{r} - \mathbf{r}'). \quad (14)$$

For instance, $\omega_3(\mathbf{r}) = \Theta(R - |\mathbf{r}|)$ characterizes the volume of a sphere. For a more detailed introduction to FMT see Ref. [7]. The extension of the bonding contribution to the inhomogeneous fluid $\Phi_{\text{bond}}(\{n_\alpha\})$ is given by a weighted-density approximation of Eqs. (6), (7), and (8). Specifically, the contact value for hard spheres is generalized to [39]

$$g_{\text{hs}}(\{n_\alpha\}) = \frac{1}{1 - n_3} + \frac{\sigma n_2 \xi}{4(1 - n_3)^2} + \frac{\sigma^2 n_2^2 \xi}{72(1 - n_3)^3}, \quad (15)$$

with $\xi = 1 - \mathbf{n}_2 \cdot \mathbf{n}_2/n_2^2$. Moreover, the bulk density ρ is replaced with $\rho \to n_0$. Since the FMT formulation of bonding has shown to give most reliable results for $M = 4$ patches, we restrict our studies to this case (cf. discussions in Sec. I or, e.g., in Sec. IV of Ref. [50]).

C. Static structure factor $S(k)$ and λ line

From previous studies of fluids with competing interactions it is well known that the static structure $S(k)$ factor plays a major role when determining the regions within the phase diagram (e.g. in the T-ρ-plane) where ordered density modulations are present [13–15,18]. These are manifested by a diverging peak at a nonzero wave number $0 < k_c \ll 2\pi/\sigma$ in $S(k)$ indicating an instability of the homogeneous bulk state with respect to periodic density modulations with a length scale $L_c \sim 2\pi/k_c$. The boundary where $S(k_c)$ diverges is referred to as the λ line.

Furthermore, when approaching the λ line, a large but finite peak in $S(k)$ at $k = k_c$ can evolve, which can be related to the onset of unordered particle clusters [23]. Recall also that the spinodal, which defines the locus in the phase diagram where a macroscopic phase separation into a gas and a liquid inevitably occurs, is obtained where $S(k)$ diverges at $k = 0$.

It follows from the Ornstein-Zernicke relation that $S(k)$ is related to the Fourier transform of the bulk pair direct correlation function $c(r)$

$$S(k) = \frac{1}{1 - \rho\,\widehat{c}(k)}, \qquad (16)$$

where $\widehat{f}(\mathbf{k}) = \int d\mathbf{r} \exp(-i\mathbf{k} \cdot \mathbf{r}) f(\mathbf{r})$ denotes the three-dimensional spatial Fourier transform of a function $f(\mathbf{r})$. In particular, $c(r)$ can be extracted from DFT by taking the second functional derivative of the excess free energy functional [1]

$$c(\mathbf{r},\mathbf{r}') = c(r = |\mathbf{r} - \mathbf{r}'|) = -\frac{\delta^2 \beta F_{\mathrm{ex}}[\rho]}{\delta\rho(\mathbf{r})\delta\rho(\mathbf{r}')}\bigg|_{\rho(\mathbf{r})=\rho}. \qquad (17)$$

Fortunately, the internal structure of FMT together with the mean-field functional allow for an analytic solution for $\hat{c}(k)$

$$\widehat{c}(k) = \widehat{c}_{\mathrm{hs}}(k) + \widehat{c}_{\mathrm{bond}}(k) + \widehat{c}_{\mathrm{r}}(k),$$

where

$$\widehat{c}(k) - \widehat{c}_{\mathrm{r}}(k) = -\sum_{\alpha,\beta} \frac{\partial^2(\Phi_{\mathrm{hs}} + \Phi_{\mathrm{bond}})}{\partial n_\alpha \partial n_\beta}\bigg|_\rho \widehat{\omega}_\alpha(\mathbf{k}) \cdot \widehat{\omega}_\beta(-\mathbf{k}) \qquad (18)$$

and

$$\widehat{c}_{\mathrm{r}}(k) = -\beta\widehat{\phi}_{\mathrm{r}}(k)$$
$$= -\frac{4\pi\beta B\sigma^3}{(k\sigma)^2 + z^2}\left[\cos(k\sigma) + \frac{z}{k\sigma}\sin(k\sigma)\right]. \qquad (19)$$

Here the $\widehat{\omega}_\alpha(\mathbf{k})$ are the Fourier-transforms of the FMT-type weight functions $\omega_\alpha(\mathbf{r})$, which are known analytically [51]. Furthermore, the partial derivatives of Φ_{hs} and Φ_{bond} can be carried out also analytically.

Equation (19) is the well-known random-phase approximation (RPA), and it is important to note that the structure factor obtained from Eqs. (16)–(19) may not equal the result obtained via the so-called test particle route [52]. In the latter, $S(k) = 1 + \rho\widehat{h}(k)$ is determined from the Fourier transform of the total pair correlation function $h(r) = g(r) - 1$, which can readily be calculated within DFT. However, we have verified that the region enclosed by the λ line obtained via Eqs. (16)–(19) and the appearance of periodic microphases via the test particle route are consistent (cf. Sec. IV).

III. BULK PHASE DIAGRAMS

In this section, we show and discuss results for the gas-liquid binodals as well as the λ line for particles with $M = 4$ patches. Liquid-gas coexistence is determined by demanding chemical and mechanical equilibrium, and the critical points are calculated by demanding that the first and second derivatives of the systems pressure p w.r.t the density ρ vanish. Diagrams are displayed in the T^*-η plane, where $T^* = k_B T/\varepsilon$. Note that we fix the amplitude ratio between attraction and repulsion, i.e., we assume $B = A\varepsilon$ as
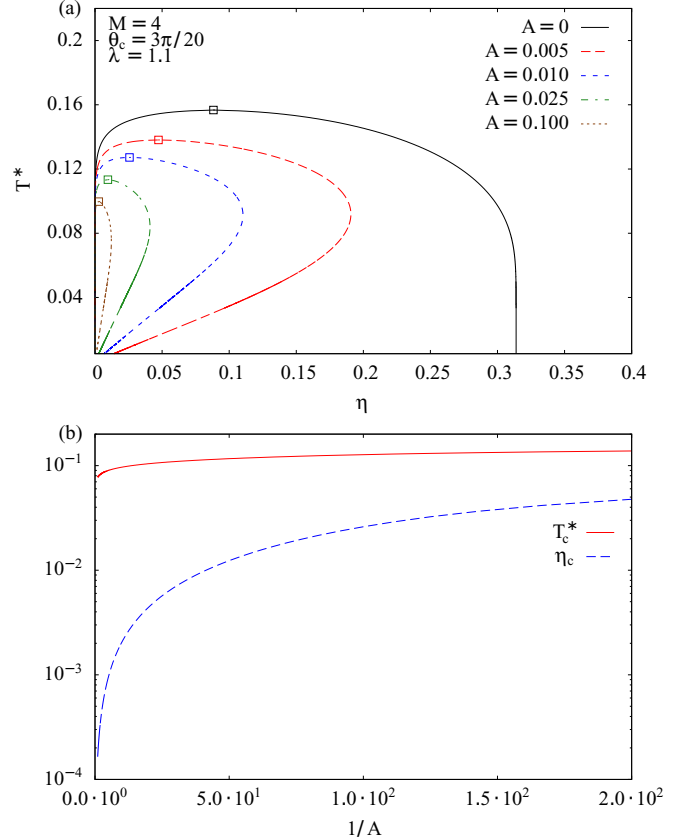
FIG. 2. (a) Gas-liquid coexistence phase diagrams in the T^*-η plane for $A = 0.005$ (red long-dashed), 0.01 (blue short-dashed), 0.025 (green dashed-dotted), and 0.1 (brown dotted). Squares denote the critical points. (b) Critical temperature T_c^* and density η_c as a function of $1/A$.

in Ref. [19], where A is a dimensionless scaling factor. It is interesting to note that while short-ranged isotropic ("sticky") potentials tend to render fully meta-stable gas-liquid binodals w.r.t gas-solid transitions, finite-valence patchy particles can yield stable gas-liquid binodals and gel-like structures on the liquid-side of the binodal despite the short range of the potential even at extreme low temperatures [53,54].

A. Gas-liquid phase separation

In Fig. 2(a) we show results for liquid-gas binodals (lines) and critical temperatures (open squares) for distinct values of A. We display curves for $A = 0$ (black solid), $A = 0.005$ (red long-dashed), 0.01 (blue short-dashed), 0.025 (green dashed-dotted), and 0.1 (brown dotted). The value of z is fixed at 0.5 which is inspired by previous DFT studies of competing interactions [15,19]. For $A = 0$, the liquid state is a gel-like percolated network mainly consisting of branched treelike structures, and a large number of patches are bonded which can be concluded by employing Flory-Stockmeyer theory [55,56] providing a percolation threshold in terms of the number of unbonded patches X [cf. Eq. (7)]. In contrast, the vapor consists of short chains or free particles, with a high probability of finding an unbonded site. When considering particles having different types of patches or mixtures with distinct numbers

of patches, Wertheim's theory predicts a rich phase behavior including reentrant liquid-gas binodals [36] and liquid states at extremely low packing fractions referred to as "empty liquids" [34]; note that all these effects are (at least qualitatively) confirmed by computer simulations.

However, we observe that the topology of the gas-liquid binodals fundamentally changes when including a long-ranged isotropic repulsion. In all cases, the liquid branch moves to significantly lower densities. As the repulsion becomes infinitely strong relative to the attraction (i.e., $1/A \to 0$), both the critical packing fraction η_c and temperature T_c^* decrease and finally vanish with a critical behavior; see Fig. 2(b). Moreover, we obtain a reentrant effect on the liquid side, i.e., when lowering the temperature at constant ρ (or, equally at constant η) at some point one enters the metastable two-phase region and subsequently reenters a stable liquid state. For the present model the effects leading to a pinched phase diagram can be understood as the result of a competition between bond formation and the isotropic repulsion. Upon cooling, repulsion influences bond formation between particles increasingly, due to the long-range character of the interaction; in order to minimize configurational energy, particles may tend to form more chainlike rather than treelike structures. As a result, with decreasing temperature, the phase-separated regime appears to shrink and vanishes for $T^* \to 0$, since a fluid of chains is known to not phase separate [34]. Moreover, statistically it gets more unlikely that a particle falls short of a center-to-center distance $\sim 1.1\sigma$ that is necessary for bonding and is orientated correctly (note that a patch covers only $\sim 5\%$ of the particles surface for the model parameters chosen in this work). This physical picture is also consistent with the observed vanishing of the critical point and shrinking of the liquid branch when increasing the repulsion relative to the bonding energy (i.e., increasing A). In particular, we have verified that the reentrant effect is no longer present in case of that the repulsion amplitude B becomes temperature independent (not shown here), but the critical point still vanishes for $B \to \infty$.

Note that from a technical point of view the reentrant effect and vanishing of the critical point are the result of a competition between the complex density dependence of Eqs. (6) and (7) and the mean-field free energy accounting for the repulsion, which scales with $\sim\rho^2$. It therefore remains an open question to what extent a theory describing the repulsion beyond the mean field would impact the phase behavior. It is also interesting to note that these effects bear a resemblance to the phase behavior of systems with so-called $2AnB$ patchy colloids [36,37]. There one places two sites of type A at the poles of each particle, and n patches of type B are placed along the equator. The particles interact via AA or via AB bonds only (with distinct interaction energies ε_{AA} and ε_{AB}), while BB bonds are forbidden. In these systems, a reentrant binodal is the result of a competition between AA bonds and AB bonds at finite temperatures if $\varepsilon_{AB} < \varepsilon_{AA}/2$.

B. Microphase separation: λ line

We now consider the λ line, which is determined by the fact that k_c is the value of k for which $S(k)$ is maximal, hence we have two equations being satisfied for $k = k_c$, namely,
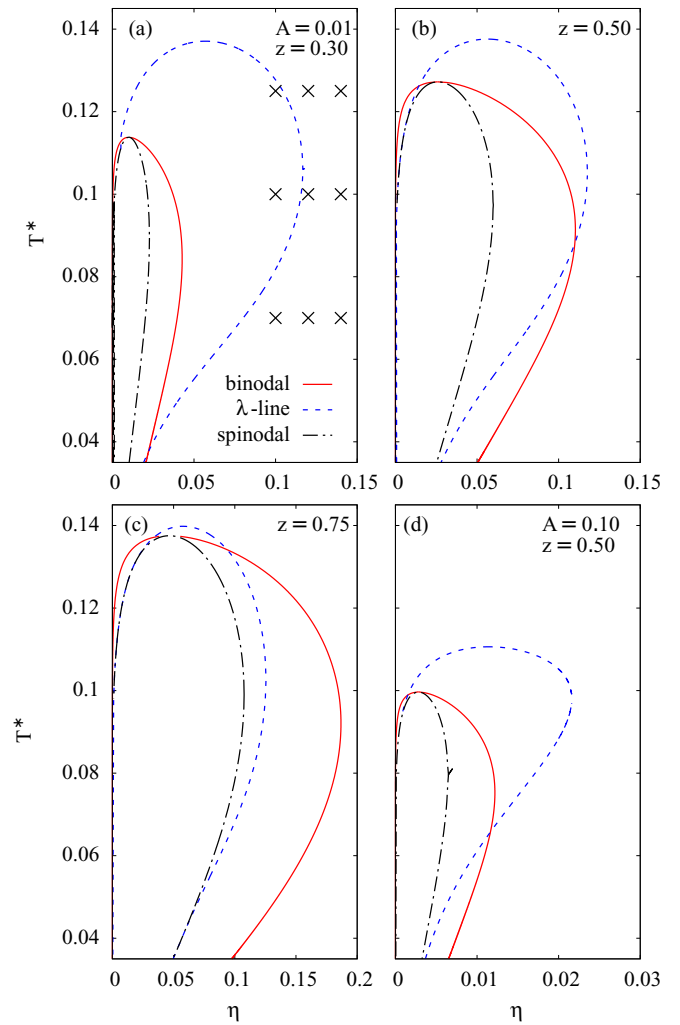
FIG. 3. (a)–(d) The binodal (red solid), spinodal (black dashed-dotted), and λ line (blue dashed) for a variety of parameters A and z. Note the small packing fractions η in (d) for $A = 0.1$ and $z = 0.5$ in comparison to $A = 0.01$ (a)–(c). Crosses in (a) denote state points shown in Fig. 5.

$D(k) \equiv 1/S(k) = 0$ and $\partial D(k)/\partial k = 0$, which we use to determine k_c and the corresponding temperature at a fixed packing fraction η.

In Figs. 3(a)–3(d) we show the λ line (blue dashed) and the respective binodal (red solid) and spinodal (black dashed-dotted) lines for a selection of parameters A and z: $A = 0.01, z = 0.3$ (a), $z = 0.5$ (b), $z = 0.75$ (c), and $A = 0.1$ and $z = 0.5$ (d). The spinodal line has been obtained using the same algorithm as we have employed for determining the λ line, albeit we searched for solutions with $k = 0$. Moreover, we have verified that the results are consistent with the compressibility route [recall that $S(k = 0) = k_B T \rho \chi_T$ where χ_T denotes the isothermal compressibility].

Strikingly, the λ line also shows a reentrant topology which is fundamentally different from spherically symmetric competing interactions [15,18,19]. For a general comparison, in Fig. 4 we show the typical phase diagram of a double-Yukawa fluid as obtained from a complete mean-field treatment of the non-hard-sphere interactions, which has been employed
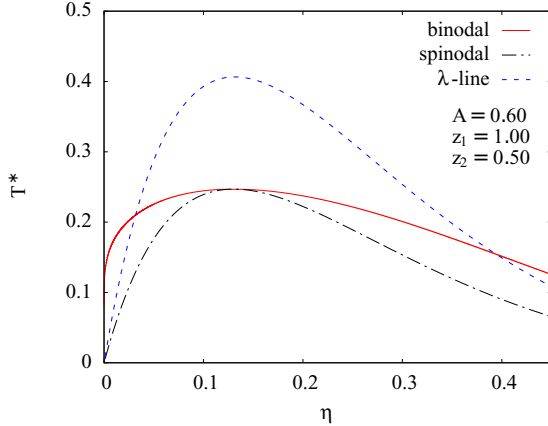
FIG. 4. Typical phase diagram of a double-Yukawa fluid as born out by a mean-field DFT treatment of the attraction and repulsion. Shown are binodal (solid), spinodal (dashed-dotted), and the λ line.

extensively in previous DFT studies [15,18,19]. Specifically, the potential is given by

$$\phi(r) = \varepsilon \left(-\frac{\sigma}{r} e^{-z_1 r/\sigma} + \frac{A\sigma}{r} e^{-z_2 r/\sigma} \right), \quad (20)$$

in which z_1 (z_2) controls the range of attraction (repulsion) and A fixes the amplitude ratio. Note that within a full mean-field treatment, the attraction needs to be significantly longer ranged in order to obtain microphase-separated states than is the case for the patchy interaction. It therefore would be an interesting future task to compare a spherically symmetric sticky attraction, which properly can be treated within FMT [57], to the present results.

A feature satisfied by both the present system and double-Yukawa fluid is that the λ line converges to the spinodal for $T^* \to 0$ on the liquid side, which here gives rise to the reentrant behavior of the λ line. For the isotropic system, however, the λ line converges to the spinodal on the vapor side also for $T^* \to 0$ (which we find to be true for all values of z_1, z_2, and A leading to microphase-separated states), while this is not the case for the present system. In particular, the λ line mainly is located on the liquid side of the phase diagram where one expects that the particles exhibit branched-like structures, and converges to the spinodal on the vapor side rather close to the critical point. This may be due to the fact that a fluid prevalently consisting of chains (as present on the vapor side of the phase diagram) seems to be incommensurate with self-assembly into complex microphases. Hence, the reentrant topology is most likely the consequence of the directionality of the interaction.

Physically, the convergence to the spinodal means that the length scales of clusters can become macroscopically large [since the wave numbers k_c associated with the divergence in $S(k_c)$ become smaller], and system-spanning cluster states can form. By altering the tuple (A, z), it is possible to greatly tune the absolute location of the λ line in the phase diagram, as well as its location relative to the binodal. When keeping A constant and varying z, the absolute extension of the λ line changes only slightly, while the binodal (and spinodal, respectively) grows clearly when reducing the range of repulsion [compare

Figs. 3(a), 3(b), and 3(c)]. However, when altering A and keeping z fixed [see Figs. 3(b) where $A = 0.01$ and 3(d) where $A = 0.1$], we see that both the liquid-gas separation as well as the region dominated by microphases can be changed on an absolute scale, whereas their relative location to each other is not affected too strongly. In particular, the theory predicts inhomogeneous bulk phases at extremely low (reservoir) packing fractions, which is consistent with our previous arguments concerning the vanishing of the critical point as the repulsion becomes increasingly dominant; as mentioned above, we expect a fluid prevalently consisting of linear chains to be unable to self-assembly into complex cluster phases.

IV. STRUCTURAL PROPERTIES

In this section we put our focus on the (bulk) structural properties of the present model system. More precisely, we calculate the fluid structure of the system around a purely repulsive test particle. Note that strictly speaking this situation does not correspond to the radial distribution function $g(r)$, but it captures the interparticle correlation effects of the surrounding fluid. In order to obtain the (orientational averaged) density distribution, we minimize the grand potential $\Omega[\rho]$ in radial symmetry w.r.t. to the density profile $\rho(\mathbf{r}) = \rho(r)$ using a standard numerical minimization scheme [7]. The potential $V_{\text{ext}}(r)$ exerted by the test particle to the surrounding fluid is given by

$$V_{\text{ext}}(r) = \begin{cases} \infty; & r < \sigma \\ \frac{A\varepsilon\sigma}{r} \exp\left[-z(r/\sigma - 1)\right]; & r \geqslant \sigma \end{cases}. \quad (21)$$

In Figs. 5(a)–5(c) we show the resulting density profiles for several values of $k_B T/\varepsilon = 0.13$ (a), 0.10 (b), and 0.06 (c) at constant packing fractions $\eta = 0.14$ (black solid), 0.12 (red dotted), and 0.10 (blue dashed). The potential parameters are $A = 0.01$ and $z = 0.3$, corresponding to the phase diagram in Fig. 3(a), where the state points are marked with crosses. For $\eta = 0.10$, the state points displayed in Figs. 5(a) and 5(b) are located inside the λ line. Here we obtain a strong radial-symmetric periodic modulation of the density $\rho(r)$. The length scale of the modulations is about roughly $L_c \approx 7$–8σ, and, in particular, the density peaks are not decaying with increasing distance to the test particle, indicating (bulk) microphase separation. Note that the respective value of the wave number where $S(k_c)$ diverges is $k_c\sigma \approx 0.8$, which is commensurate with the obtained periodicity of the density.

For densities $\eta = 0.12$ and 0.14, the state points are in vicinity to but outside the λ line, and here we observe that long-ranged slowly decaying cluster correlations are emerging. These may be related to unordered cluster phases, which in a bulk situation would be not recognizable [i.e., on statistical average the system shows a bulk state with $\rho(\mathbf{r}) = \text{const}$], in contrast to ordered microphases inside the λ line. These decaying cluster correlations can be related to a large but finite peak in $S(k)$ at $k = k_c$ [23,58,59], and they pass over to a complete periodic modulated density when approaching the λ line where $S(k)$ divergences at $k = k_c$ (e.g., by following a path at constant T^*). In particular, the oscillations reflect the reentrant topology of the phase diagrams: far from the λ line [cf. Fig. 5(a)] only weak oscillations can be seen; in its direct
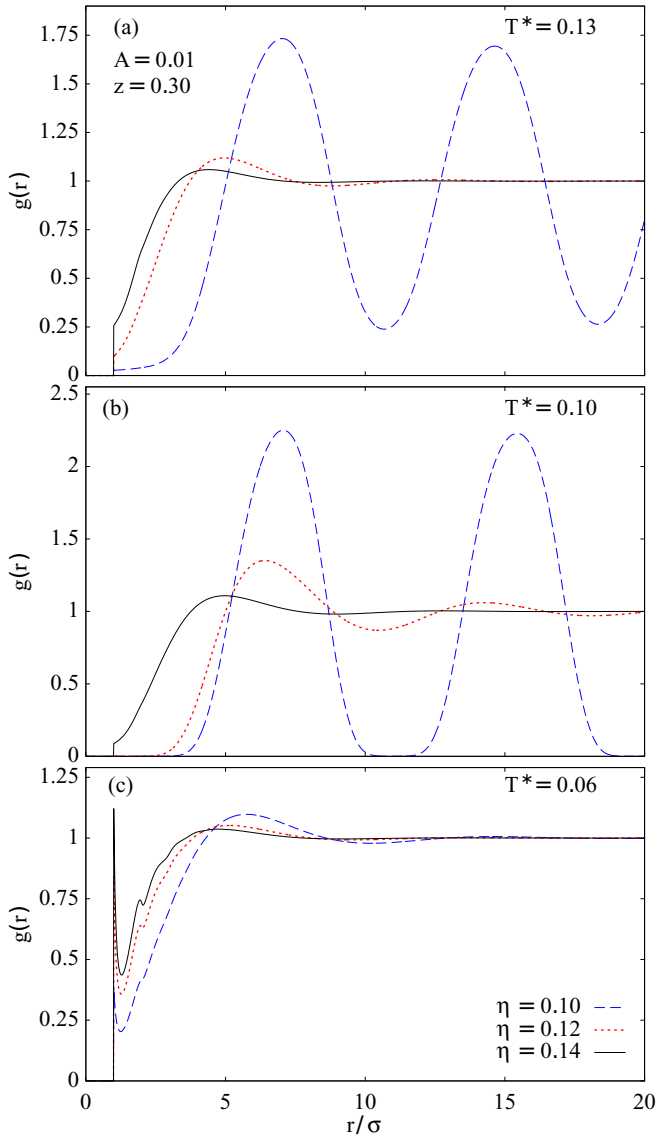
FIG. 5. Radial distribution function $g(r)$ around a purely repulsive test particle for different values $T^* = 0.13$ (a), 0.10 (b), and 0.06 (c), and packing fractions $\eta = 0.10$ (blue dashed), 0.12 (red dotted), and 0.14 (black solid). The potential parameters correspond to the phase diagram in Fig. 3(a), where the state points are marked with crosses.

vicinity, cluster correlations are clearly visible, in particular for $\eta = 0.12$. By further decreasing temperature [Fig. 5(c)] cluster correlations in turn become less pronounced.

V. INHOMOGENEOUS BULK PHASES

We now discuss what kind of bulk microphases can be stable within the region enclosed by the λ line. Considering the complex phase behavior of the present system, the question arises how the typical sequence of 3D structures, namely, bcc-2D-hexagonal-gyroid-lamellar-inverted gyroid-inverted 2D-hexagonal-inverted bcc predicted by Landau-type theories and full DFT-calculations [12,19] for systems with spherically competing interactions may be affected by an anisotropic

attraction. Note that this ordering of structures is also observed experimentally in diblock copolymers [9].

To this end, we go along the lines of Ref. [19] in order to find the microphase with the lowest configurational energy, which within the framework of DFT can be obtained by considering the value of the grand potential functional $\Omega = \Omega[\rho_0(\mathbf{r})]$ evaluated at the density distribution describing a specific structure. Recall that within the λ line, the homogeneous bulk phase, i.e., $\rho(\mathbf{r}) = \rho = \text{const}$ is unstable w.r.t *any* arbitrary small perturbation $\rho(\mathbf{r}) = \rho + \delta\rho(\mathbf{r})$. In particular, the free-energy landscape can be very complex: if $\delta\rho(\mathbf{r})$ is a random noise term, typically one ends up with an arbitrary periodic intermediate structure which is commensurate with the size of the unit cell and usually does not correspond to a global minimum of the system. Hence, in order to determine the structures with lowest energy, the perturbation $\delta\rho(\mathbf{r})$ must be chosen properly close to the desired structure, otherwise numerical schemes used to minimize Eq. (9) may run into local minima representing metastable states [19]. Note that $\Omega[\rho]$ must also be minimized with respect to the size of the unitcell L, which makes the calculation of certain structures numerically challenging and leads to huge computational effort. In order to obtain a reasonable balance between computation time and accuracy of the results, here we make use of a massively parallel minimization on GPUs [60]. For certain symmetry groups (e.g., $Im\bar{3}m, Fm\bar{3}m$) one can make use of Fourier expansions, and in many cases it suffices to employ the respective first-order approximation. For instance, the perturbation term describing the lamellar phase is given by $\delta\rho_{\text{lam}}(\mathbf{r}) = \gamma\sqrt{2}\cos(2\pi k_c x/L)$, where γ controls the strength of the perturbation. Further structures can be found in Ref. [61].

Note that an order-parameter theory, which qualitatively predicts different types of stable microphases, readily can be derived for a local density approximation (LDA) of the hard-sphere correlations and a full mean-field treatment of the longer-ranged interactions [18,19]. However, for the present system this is very cumbersome due to the full FMT-type character of the attraction, and a LDA treatment of the Wertheim theory is not capable of predicting a λ line, because the respective $\hat{c}_{\text{bond}}$ does not posses a dependency on the wave vector k, which is mandatory for obtaining a diverging peak in $S(k)$.

We plot in Fig. 6 structures from several symmetry groups that according to the present theory can exist as stable microphases, which includes a double-gyroid (a), 2D-hexagonal (b), and a bcc structure (c), or at least as metastable phases such as the single-gyroid (d). Considering the size L of the individual unit cells, we find that for state points located well inside the λ line, they range between $\approx 20–30\sigma$ for the double-gyroid, $\approx 12–20\sigma$ for, e.g., the bcc- or single-gyroid structure, and $\approx 7–12\sigma$ for the lamellar phase. Note that in general the Fourier expansions of specific structures depend also on the miller indices $\{hkl\}$, and the associated theoretical length scales of these structures are related to the wave number k_c via

$$L_c = \frac{2\pi}{k_c}\sqrt{h^2 + k^2 + l^2}. \tag{22}$$

The actual sizes of the unit cells found by minimization of the grand potential are in good agreement with
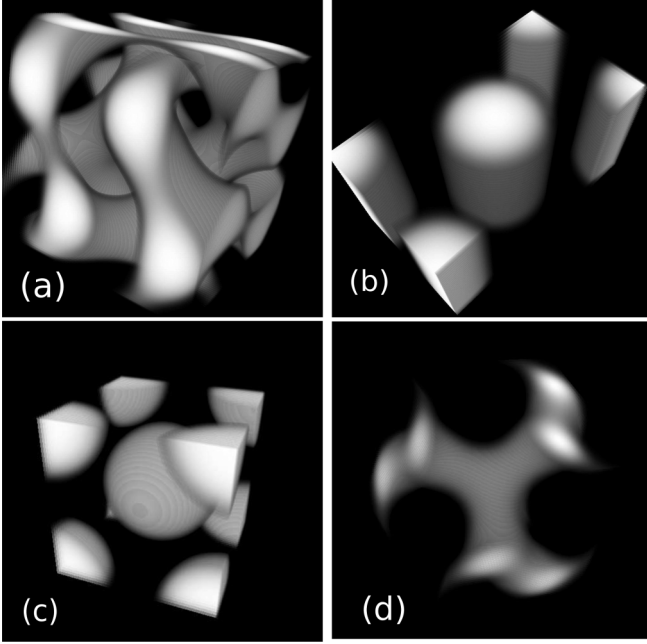
FIG. 6. A double-gyroid (a), 2D hexagonal (b), bcc (c), and single-gyroid phase (d) predicted by the present DFT. All but the single-gyroid phase can exist as stable phases, and these structures also have been observed in DFT and Monte Carlo simulation studies using spherically competing interactions [19,20].

Eq. (22). Remarkably the size of the unit cell does not qualitatively depend on the phase diagrams [cf. Figs. 3(b) and 3(c)], although the (reservoir) particle densities differ by nearly an order of magnitude. Moreover, the values of L are very similar to the case of spherically competing interactions [19].

It is interesting to note that self-assembly into complex structures including gyroid phases can be observed in biologic processes of some animals: There they form photonic crystals, e.g., in bird feathers [24] or butterfly wings [25], and these are responsible for structural coloring, i.e., wavelength-selective scattering of visible light. This means that the length scale of these structures is within the range $\sim$300–600 nm, and, strikingly, assuming an effective particle diameter of $\sim$10–20 nm which is the typical length scale of proteins or complex polymers, the respective sizes of the unit cells observed in systems with competing interactions match the scale corresponding to the wavelength of visible light. In particular, the effects behind the self-assembly into biophotonic nanostructures were suggested to be driven by a thermodynamic phase separation [24].

In Fig. 7(a) we show $\Omega/|\Omega_l|$ normalized w.r.t the absolute value of the lamellar phase Ω_l as a function of the reservoir packing fraction η for $T^* = 0.12$, $A = 0.01$, and $z = 0.3$, corresponding to the phase diagram shown in Fig. 3(a). Essentially, for these parameters we observe the same ordering of structures as predicted for spherically competing interactions: bcc-2D-hexagonal-gyroid-lamellar-inverted gyroid-inverted 2D-hexagonal-inverted bcc. For readability of the plot the bcc phase is not pictured, as it occurs only in direct vicinity to the λ line. The kinks in the graphs indicate
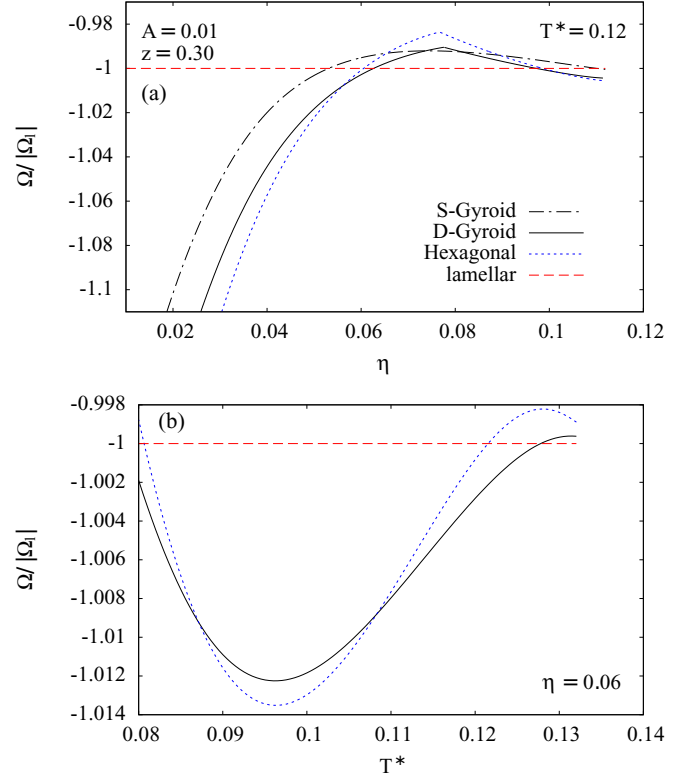
FIG. 7. (a) The grand potential Ω normalized w.r.t. the lamellar phase (red dashed line) as a function of η at $T^* = 0.12$ for structures with lowest free energies, including a single gyroid (green dashed-dotted), double gyroid (black solid), and 2D hexagonal phase (blue dotted). (b) Same as in (a) but as a function of T^* for fixed $\eta = 0.06$.

a first-order transition to the inverted structure, i.e., where low-density and high-density domains are exchanged. Note that, e.g., the lamellar or the single-gyroid structure is its own inverse, and hence the related curves are smooth functions of η. Figure 7(b) pictures the same as in Fig. 7(a) but for a function of T^* at fixed $\eta = 0.06$, where we observe a reentrant effect: starting from a stable lamellar structure, the gyroid phase becomes stable between $T^* \approx 0.127$ and $T^* \approx 0.11$. Subsequently, this is followed by a region where the 2D-hexagonal structure corresponds to the global minimum, and at $T^* \approx 0.09$ the gyroid becomes the most stable structure again. For even lower temperatures, approaching the λ line, again the lamellar phase is stable. This behavior directly reflects the topology of the λ line and is not compatible with the typical phase diagrams in systems with spherically competing interactions [12,19]. We have performed the same calculations also for the phase diagram in Fig. 3(d) and found a similar behavior: although here the inverse structures (e.g., inverse double-gyroid or bcc) seem to be unstable [despite a properly chosen initial perturbation $\delta\rho(\mathbf{r})$ one ends up with an intermediate microstructure], which may be due to the fact that the packing fraction is too low in order to generate these structures. It remains an interesting future task to completely sample through the phase diagrams pictured in Figs. 3(a)–3(d) and determine the concrete ordering of structures, which, however, goes beyond the scope of the current work.

VI. SUMMARY AND CONCLUSION

In this paper we presented a DFT study investigating systems with competing interactions, where the constituents undergo a short-ranged patchy attraction via four equal interactions sites on their surface and a spherical long-ranged repulsion. While the anisotropic interaction is accounted for within Wertheim's first order perturbation theory (TPT1) [33] and a generalization to nonhomogeneous situations as proposed by Yu and Wu [39] within the framework of FMT, the repulsion is treated in a standard mean-field manner.

We calculated the respective gas-liquid coexistence regions, as well as the λ line which encloses a region in the phase diagram where the bulk fluid becomes unstable w.r.t to fluctuations and self-assembles into (periodic) microphases, which is a well-known phenomenon in systems with spherical competing interactions; see, e.g., Refs. [12,15,19,20] and references therein. Importantly, the topology of the phase behavior fundamentally changes in comparison to spherically symmetric interactions: The diagrams feature phenomena such as vanishing critical points and reentrant behavior, which are reminiscent of systems consisting of pure patchy colloids with two distinct types of patches per particles [36]. In our case, the observed behavior can be understood by the interplay of bond formation and effects of repulsion; see discussions given in Sec. III A. In Sec. IV we calculated the density profile $\rho(r)$ around a repulsive test particle having the same geometrical size as the surrounding particles. Here we find that the bulk behavior of the system is clearly reflected in the structure of the fluid; reentrant cluster correlations in $g(r)$ are visible along a path of constant density in vicinity to the λ line. Subsequently, in Sec. V we investigated what kind of microphases can be stable within the λ line, and we found that in principal the same structures are predicted as in systems with spherically competing interactions. In particular, complex structures such as the double gyroid can be stable also at extremely low reservoir packing fractions $\eta \sim 0.01$.

One may raise concerns about that the mean-field approach employed to model the repulsive contribution as well as the treatment of the patchy attraction applied in this work allow only for rough conclusions. However, we expect our results to be at least qualitatively reliable. First, Archer and Evans recently have shown for one-dimensional attractive rods, where an exact approach is available, that the corresponding mean-field DFT is in reasonable good agreement with the exact solution [52]. Moreover, previous mean-field DFT studies of isotropic competing interactions have predicted complex three-dimensional microphases including fcc- and double-gyroid structures in good agreement with simulations, even in terms of the topology of the λ line [19,20]. Moreover, the appearance of a large but finite peak in $S(k)$ has been interpreted as the onset of clustering in various simulation studies by considering the peak height and width [58,59], which is consistent with previous mean-field descriptions and our present findings regarding the density profiles shown in Sec. IV. In addition, although Wertheim's theory is known to underestimate the bulk phase diagrams at higher densities [36], it qualitatively captures essential effects compared to simulations.

Finally, it is worth noting that the investigated system may serve as a toy model for protein-salt mixtures in aqueous solution [30,62]. In these systems, multivalent salt ions can bind to the surface of globular proteins and induce highly directional bonds between the proteins, which for sufficient salt concentrations results in reentrant protein clustering and a closed-loop liquid-liquid phase separation (LLPS) region, i.e., phase separation into protein-poor and protein-rich regions [62]. In a recent work, Roosen-Runge *et al.* have developed an appealing theory using TPT1 in order to model the ion-activated interaction between proteins. While the LLPS is accurately reproduced by the approach which does not take into account electrostatics explicitly, open questions remain regarding experimentally observed large protein clusters. Thus, taking into account electrostatic interactions in terms of a screened Coulomb potential seems a natural next step for improving the model [30]. In particular, the observed clustering at very low protein packing fractions is compatible with the present system, where unordered cluster phases and microphases can occur at very low packing fractions.

[1] J.-P. Hansen and I. McDonald, *Theory of Simple Liquids*, 4th ed. (Academic Press, London, 2013).

[2] J. K. Percus and G. J. Yevick, Phys. Rev. **110**, 1 (1958).

[3] J. L. Lebowitz, Phys. Rev. **133**, A895 (1964).

[4] R. L. Davidchack, B. B. Laird, and R. Roth, Condens. Matter Phys. **19**, 23001 (2016).

[5] R. Evans, Adv. Phys. **28**, 143 (1979).

[6] Y. Rosenfeld, Phys. Rev. Lett. **63**, 980 (1989).

[7] R. Roth, J. Phys.: Condens. Matter **22**, 063102 (2010).

[8] P. Tarazona and R. Evans, Mol. Phys. **48**, 799 (1983).

[9] S. Foerster, A. K. Khandpur, J. Zhao, F. S. Bates, I. W. Hamley, A. J. Ryan, and W. Bras, Macromolecules **27**, 6922 (1994).

[10] M. W. Matsen and M. Schick, Phys. Rev. Lett. **72**, 2660 (1994).

[11] V. E. Podneks and I. W. Hamley, JETP Lett. **64**, 617 (1996).

[12] A. Ciach, Phys. Rev. E **78**, 061505 (2008).

[13] R. P. Sear and W. M. Gelbart, J. Chem. Phys. **110**, 4582 (1999).

[14] A. Imperio and L. Reatto, J. Phys.: Condens. Matter **16**, S3769 (2004).

[15] A. J. Archer, D. Pini, R. Evans, and L. Reatto, J. Chem. Phys. **126**, 014104 (2007).

[16] E.-Y. Kim, S.-C. Kim, and S.-H. Suh, Phys. Rev. E **85**, 051203 (2012).

[17] A. J. Archer and N. B. Wilding, Phys. Rev. E **76**, 031501 (2007).

[18] A. J. Archer, C. Ionescu, D. Pini, and L. Reatto, J. Phys.: Condens. Matter **20**, 415106 (2008).

[19] M. Edelmann and R. Roth, Phys. Rev. E **93**, 062146 (2016).

[20] Y. Zhuang, K. Zhang, and P. Charbonneau, Phys. Rev. Lett. **116**, 098301 (2016).

[21] R. Roth, Mol. Phys. **109**, 2897 (2011).

[22] D. Pini, A. Parola, and L. Reatto, J. Chem. Phys. **143**, 034902 (2015).

[23] Y. Zhuang and P. Charbonneau, J. Phys. Chem. B **120**, 7775 (2016).

[24] E. R. Dufresne, H. Noh, V. Saranathan, S. G. J. Mochrie, H. Cao, and R. O. Prum, Soft Matter **5**, 1792 (2009).

[25] V. Saranathan, C. O. Osuji, S. G. J. Mochrie, H. Noh, S. Narayanan, A. Sandy, E. R. Dufresne, and R. O. Prum, Proc. Natl. Acad. Sci. USA **107**, 11676 (2010).

[26] H. Liu, S. K. Kumar, and F. Sciortino, J. Chem. Phys. **127**, 084902 (2007).

[27] D. Fusco and P. Charbonneau, Phys. Rev. E **88**, 012721 (2013).

[28] C. Gögelein, G. Nägele, R. Tuinier, T. Gibaud, A. Stradner, and P. Schurtenberger, J. Chem. Phys. **129**, 085102 (2008).

[29] B. Ruzicka, E. Zaccarelli, L. Zulian, R. Angelini, M. Sztucki, A. Moussaid, T. Narayanan, and F. Sciortino, Nat. Mater. **10**, 56 (2011).

[30] F. Roosen-Runge, F. Zhang, F. Schreiber, and R. Roth, Sci. Rep. **4**, 7016 (2014).

[31] P. Teixeira and J. Tavares, Curr. Op. Coll. Int. Sci. **30**, 16 (2017).

[32] M. Wertheim, J. Stat. Phys. **35**, 19 (1984).

[33] G. Jackson, W. Chapman, and K. Gubbins, Mol. Phys. **65**, 1 (1988).

[34] E. Bianchi, J. Largo, P. Tartaglia, E. Zaccarelli, and F. Sciortino, Phys. Rev. Lett. **97**, 168301 (2006).

[35] D. de las Heras, J. M. Tavares, and M. M. T. da Gama, J. Chem. Phys. **134**, 104904 (2011).

[36] J. Russo, J. M. Tavares, P. I. C. Teixeira, M. M. Telo da Gama, and F. Sciortino, Phys. Rev. Lett. **106**, 085703 (2011).

[37] J. Russo, J. M. Tavares, P. I. C. Teixeira, M. M. T. da Gama, and F. Sciortino, J. Chem. Phys. **135**, 034501 (2011).

[38] C. J. Segura, W. G. Chapman, and K. P. Shukla, Mol. Phys. **90**, 759 (1997).

[39] Y.-X. Yu and J. Wu, J. Chem. Phys. **116**, 7094 (2002).

[40] A. Oleksy and P. I. C. Teixeira, Phys. Rev. E **91**, 012301 (2015).

[41] S. Sokołowski and Y. V. Kalyuzhnyi, J. Phys. Chem. B **118**, 9076 (2014).

[42] J. Hughes, E. J. Krebs, and D. Roundy, J. Chem. Phys. **138**, 024509 (2013).

[43] N. Gnan, D. de las Heras, J. M. Tavares, M. M. T. da Gama, and F. Sciortino, J. Chem. Phys. **137**, 084704 (2012).

[44] N. Kern and D. Frenkel, J. Chem. Phys. **118**, 9882 (2003).

[45] M. Wertheim, J. Stat. Phys. **35**, 35 (1984).

[46] M. Wertheim, J. Stat. Phys. **42**, 459 (1986).

[47] M. Wertheim, J. Stat. Phys. **42**, 477 (1986).

[48] Y. Tang, Y.-Z. Lin, and Y.-G. Li, J. Chem. Phys. **122**, 184505 (2005).

[49] H. Hansen-Goos and R. Roth, J. Phys.: Condens. Matter **18**, 8413 (2006).

[50] D. de las Heras and M. M. T. da Gama, J. Phys.: Condens. Matter **28**, 244008 (2016).

[51] Y. Rosenfeld, Phys. Rev. A **42**, 5978 (1990).

[52] A. J. Archer, B. Chacko, and R. Evans, J. Chem. Phys. **147**, 034501 (2017).

[53] F. Smallenburg and F. Sciortino, Nat. Phys. **9**, 554 (2013).

[54] F. Sciortino and E. Zaccarelli, Curr. Op. Coll. Int. Sci. **30**, 90 (2017).

[55] P. Flory, J. Am. Chem. Soc. **63**, 3083 (1941).

[56] E. Bianchi, P. Tartaglia, E. Zaccarelli, and F. Sciortino, J. Chem. Phys. **128**, 144504 (2008).

[57] H. Hansen-Goos, M. A. Miller, and J. S. Wettlaufer, Phys. Rev. Lett. **108**, 047801 (2012).

[58] N. E. Valadez-Pérez, R. Castañeda-Priego, and Y. Liu, RSC Adv. **3**, 25110 (2013).

[59] J. A. Bollinger and T. M. Truskett, J. Chem. Phys. **145**, 064902 (2016).

[60] D. Stopper and R. Roth, J. Chem. Phys. **147**, 064508 (2017).

[61] H. G. von Schnering and R. Nesper, Z. Phys. B Condens. Matter **83**, 407 (1991).

[62] F. Zhang, M. W. A. Skoda, R. M. J. Jacobs, S. Zorn, R. A. Martin, C. M. Martin, G. F. Clark, S. Weggler, A. Hildebrandt, O. Kohlbacher *et al.*, Phys. Rev. Lett. **101**, 148101 (2008).